Investigation of laser compression of shell targets

A. E. Barulin, B. I. Bayanov, V. G. Borodin, A. S. Ganeev, A. A. Gorokhov, A. L. Zapysov,
A. I. Zuev, A. F. Ivanov, I. M. Izrailev, V. M. Komarov, V. N. Korolenko,
V. I. Kryzhanovskiĭ, V. B. Kryuchenkov, V. A. Lykov, A. A. Mak, V. A. Malinov,
V. M. Migel', N. V. Nikitin, V. A. Podgornov, V. G. Pokrovskiĭ, V. A. Pronin,
V. A. Serebryakov, N. A. Solov'ev, A. D. Starikov, A. V. Charukhchev, V. N. Chernov,
A. A. Chertkov, and E. G. Sheĭkin

Experimental results are reported on spherical irradiation of gas-filled glass microspheres using the six-beam "Progress" neodymium laser device at flux densities reaching $\sim 10^{15} \text{W/cm}^2$ at the surface of the target. The experimental data are compared with numerical results calculated using the "Zarya" computer code. Optimum calculated target parameters are given for various irradiation conditions in the "Progress" device.

1. INTRODUCTION

In this paper we analyze experimental results obtained by using the six-beam "Progress" Nd laser device[1,2] to irradiate targets of the type used in laser fusion research. Optimum target and laser parameters are calculated for use in future experiments.

In our series of experiments[1] we irradiated glass microspheres uniformly with laser pulses of wavelength $\lambda_0 = 1.054 \mu\text{m}$ and duration $\tau_{1/2} = 0.2$ ns (half-maximum). The spheres, of radius $R_0 = 45$–60 μm, wall thickness $b = 0.6$–$1.2 \mu\text{m}$ and aspect ratio $R_0/b = 50$–110, were irradiated in vacuum with delivered energies $E_t = 60$–130 J and heat fluxes $q = (0.5 - 2) \cdot 10^{15}$ W/cm^2 at the target surface. The total energy contrast was $(3$–$6) \cdot 10^5$ and the thickness of the sphere walls was uniform to within $\Delta b /b = \pm (4$–$20)\%$. The laser light was focused to a distance $a = 140$–330 μm behind the center of the target, and computer calculations using the "LAST" code[3] indicated that the target was illuminated uniformly to within $\Delta\Phi/\Phi \leqslant \pm 23\%$ relative to the average value. The experiments were carried out both for empty spheres and for spheres filled with DT gas.

We used the following apparatus to measure the parameters of the laser plasma:

1) A 7-channel cw x-ray spectrometer[4] (photon energy $\varepsilon = 4$–43 keV) designed from semiconductor and scintillation detectors with selective filters (we used the K-absorption edge).

2) Vacuum x-ray diodes,[5] with a wave resistance of 50 Ω and a time resolution of between 120 and 200 ps (this was measured experimentally and includes the response time of the recording system, which contained an S7-15 oscilloscope). The vacuum diodes were used with Cu and Al filters to select the L- and the K-absorption edges, respectively.

3) A spectrometer[4] to analyze the x-ray emission lines from multiply charged Si ions. The spectrometer consisted of a planar gypsum crystal whose entrance face contained slits of width $10 \mu\text{m}$. The spectrometer enabled us to simultaneously record both the spatially averaged x-ray line intensity and pairs of two-dimensional images of the laser plasma. The latter were recorded with a spatial resolution of 15×25 μm at the wavelengths of individual x-ray lines.

4) Multichannel x-ray pinhole cameras, which were used with filters to select the K absorption edges for Al, Si, Cu, Ti, and Fe. As described in Ref. 6, the spatial resolution was 2–4 μm.

5) Faraday-cup ion collectors similar to the ones in Ref. 7.

6) A scintillation neutron detector, based on an FÉU-65 photomultiplier and a plastic scintillator of dimensions 150×100 mm, to record the neutron yield from the D-T reactions. We used a 1-cm-thick lead shield to protect the detector from the ultrahard x-rays (estimated energy $\varepsilon > 200$ KeV) observed during the experiments: alternatively the x-ray and neutron signals were separated through their transit times.

The x-ray detectors were first calibrated absolutely (see Refs. 4, 5, 8, and 9 for more details). The sensitivity of the neutron detector was calibrated in terms of a Co^{60} source and corrected using data in Ref. 10 to give the sensitivity to 14 MeV neutrons.

2. LASER PLASMA DIAGNOSTICS

The energy E_a absorbed by the target was deduced from the signals received from the ion collectors; as in Ref. 11, it was found to be 10–15% of the incident energy E_i at the target. We also measured the ratios E_x/E_a and E_{fi}/E_a, where E_x is the total energy of the hard x-rays (extrapolated as in Ref. 12 to $\varepsilon = 0$) and E_{fi} is the energy which is absorbed by the target and carried away by the fast ions. Both E_x/E_a and E_{fi}/E_a were similar to the values in Ref. 12, which indicates that as in Ref. 12, anomalous absorption was important under the experimental conditions. Table I presents values of E_i, E_a, E_x/E_a, and E_{fi}/E_a, along with calculated values for $(\Delta\Phi/\Phi)_0$ and $(\Delta\Phi/\Phi)_m$, the illumination nonuniformities initially and at the instant of peak laser pulse power. The errors in E_a and E_{fi} are equal to $\pm 25\%$ and $\pm 50\%$, respectively, while E_x is accurate to within a factor of 2.

The laser targets were imploded under conditions similar to those for "exploding" shells. We select a typical experiment (No. 78) for subsequent analysis; in this experiment the target parameters were $R_0 = 53.2 \mu\text{m}$, $b = 0.58 \mu\text{m}$, $\Delta b / b = \pm 9.8\%$, and the pressure of the DT gas was $p_{DT} = 4$

TABLE I. Measurement results.

Parameter	Experiment No.			
	78	87	89	91
E_i, J	62	106	71,5	63,4
q, W/cm^2	$5,7\cdot10^{14}$	$1,5\cdot10^{15}$	$1,5\cdot10^{15}$	$7,6\cdot10^{14}$
E_a, J	9,0	10,6	10,7	9,1
E_x/E_a	$9\cdot10^{-5}$	$5,5\cdot10^{-4}$	—	$6\cdot10^{-5}$
E_{fi}/E_a	0,12	—	0,42	0,35
a, μm	224	224	224	224
$(\Delta\Phi/\Phi)_0$	0,21	—	0,17	—
$(\Delta\Phi/\Phi)_m$	1,35	—	1,5	—

atm. The time- and space-averaged parameters of the laser plasma found in this experiment agreed with the results calculated using the "Zarya" code. In particular, the experimental value of E_a was 9 ± 3J, while the calculated value was 8.5 J. At lower energies, the experimentally recorded continuous x-ray emission spectrum (Fig. 1) is similar to the "Zarya" result, but the two diverge considerably at higher energies. We note that a similar discrepancy in the hard x-ray component is also found when the calculations are compared with experimental results obtained using other equipment (see, e.g., Ref. 13). It can be traced to the fact that the calculations treat the bremsstrahlung only for a single pass of the fast electrons across the target, whereas in the corona of the laser plasma the fast electrons give up a significant fraction of their energy to the ions only after crossing the target several dozen times.

The temperatures T_c and T_h of the thermal (cold) and hot electrons shown in Table II were deduced from the slope of the calculated and experimental spectra in Fig. 1. The calculated and experimental values agree, and they also coincide with T_c and T_h found from the experimentally recorded velocity distribution of the ions in the laser plasma.

Table II also compares calculated and experimental values for the absolute spectral line intensities (we use the standard designations for the lines[14]).
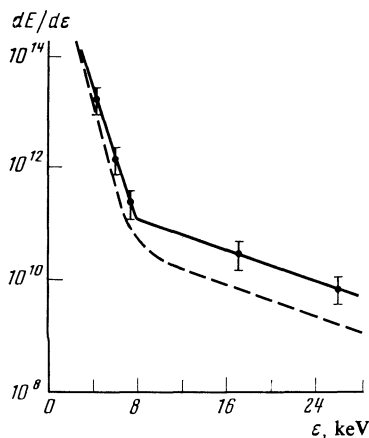
$dE/d\varepsilon$

FIG. 1. Continuous x-ray emission spectrum recorded experimentally (solid line) and calculated using the "Zarya" code (dashed line).

If we compare the experimental intensities E_{jk} and E_w with the calculated values (found by neglecting the absorption in the plasma), we see that the self-absorption is considerable (roughly tenfold) for the w line and its dielectronic satellites. The same conclusion follows if the calculated plasma temperature and density profiles are used to analyze the absorption of these lines in the emitting region of the plasma.

It was shown in Ref. 15 that when strong absorption occurs, the intensity ratio $E_{jk}/E_w \approx 0.15-0.2$ is almost independent of the electron temperature T_e for $T_a \lesssim T_e \lesssim T_b$ (our estimates for silicon give $T_a \approx 0.3$ keV, $T_b \approx 0.7$ keV). The same value of E_{jk}/E_w was found in our experiment, which provides further evidence for significant self-absorption for the w, j, and k lines.

On the other hand, if we compare the experimental and calculated intensities E_{Ly_α}, $E_{G,Q\ldots}$ for hydrogenic ions and analyze the absorption in the emitting region, we find that there was little self-absorption under our experimental conditions; moreover, the electron temperature T_e, deduced from the ratio $E_{G,Q\ldots}/E_{Ly_\alpha}$ by assuming an optically thin plasma and using the formula in Ref. 4, is equal to the electron temperature in the vaporized portion of the target. Values of T_e are presented in Table II.

We monitored the compression of the target directly in terms of the time behavior of the soft x-rays and by analyzing time-integrated two-dimensional images of the laser plasma recorded both by pinhole cameras and by the crystal spectrometer. Figure 2 shows an analysis of pinhole images of the laser plasma recorded in experiment No. 78. In all cases a bright central ring is present; we attribute it to emission from the compressed portion of the glass shell. The size of the ring agrees with the calculated values as may be seen from Fig. 3, in which results for several pinhole images recorded for filter energies $\bar\varepsilon = 2.6$ keV are averaged and compared (in absolute units) with results calculated using the "Zarya" code. The ratio of the radius of the bright ring in the pinhole image divided by the initial radius of the target yields a lower bound[2] for δ, the volume compression of the target. This value is shown in Table II, which also gives the calculated compression δ.

The images of the laser plasma recorded by the pinhole cameras and crystal spectrometer are in mutual agreement (see Fig. 4), provided we bear in mind that the photons corresponding to the discrete lines and to the continuous spectrum are emitted from different regions of the plasma (the

TABLE II. Parameters of the laser plasma in experiment no. 78.

	T_e, keV	T_c, keV		T_h, keV		E_w, mJ	E_{jk}, mJ	E_{Ly_α}, mJ	$E_{G,Q...}$, mJ	δ
		x-rays	ions	x-rays	ions					
Exper.	0,62±0,09	0,73±0,1	0,85	5,5±2	4	19,4±4	3,1±0,8	11±2,2	1,3±0,5	2400(+1200−700)
calc.	0,56	0,69	0,69	6	6	197	31	13	1,8	1500

latter photons contribute to the image in the pinhole photographs).

Figure 5 compares experimental and calculated dependences $W(\varepsilon, t)$ for the x-rays spectral power density; the calculated values $W(\varepsilon\, t)$ were corrected for the pulse characteristic. The curves were matched at 2% peak power, which is the lowest level that can be reliably analyzed on the oscilloscope traces. The arrows in Fig. 5 indicate the shell collapse time t_c, which agrees with the calculated time of peak x-rays power. The figure shows that on the whole, the calculated curve $W(\varepsilon, t)$ corrected for the pulse characteristic of the vacuum x-rays diodes in the recording system, correctly describes the experimental time dependence of the x-ray intensity, except for the last (decay) stage. The experimentally recorded delay of the trailing edge of the x-ray pulses was apparently due to recombination and line emission from the nonequilibrium expanding plasma during the stage when its ionization state was "frozen-in."

We used the crystal spectrometer to measure the continuous spectrum near the absorption edge in greater detail. Figure 6 shows the results, together with measurements found using vacuum x-rays diodes, semiconductor detectors, and pinhole cameras. We see that the various methods are in agreement to within the measurement error and give results that are adequately approximated by the solid curve,
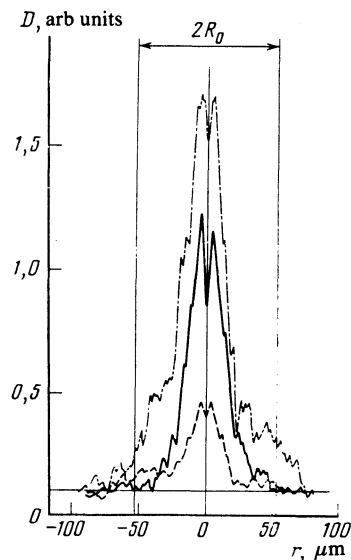
which was calculated (up to a constant) by neglecting the shift in the absorption edges and assuming a plasma with equal electron and ion temperatures and a steady-state ion composition. This agreement shows that in our experiment, the time-dependence of the ionization was relatively unimportant during the compression stage. Comparison of the experimental and calculated magnitudes of the absorption jumps shows that the concentration of hydrogen-like Si ions must have been at least 33–50% of the corresponding value for an equilibrium plasma.

Figure 6 shows that the experimental absorption jump is broadened and shifted by $\Delta\varepsilon = 100 \pm 20$ eV (half-maximum) relative to the ionization potential $\varepsilon_0 = 2.438$ keV for an isolated helium-like silicon ion. We find the value $\rho = 1$–2.7 g/cm^3 for the plasma density from the formula

$$\Delta\varepsilon \approx 26\bar{z}(\rho/\bar{A})^{0,387}, \tag{1}$$

which approximates the numerical calculations in Ref. 16 for the shift in the absorption jump for $T_e = 0.1$–0.3 keV. Here $\bar{z}$ is the average charge of the ions in the plasma, $\bar{A}$ is their average atomic weight, $\Delta\varepsilon$ is in eV, and we take $\bar{z} = 10$, $\bar{A} = 20$ (for an SiO_2 plasma), and $\Delta\varepsilon = 80$–120 eV. Numerical calculations using the "Zaray" show that photons with energies lying near the absorption edge are emitted primarily from the compressed part of the shell, where the density reaches 2–3.5 g/cm^3.

The neutron yield $N_{DT} = (7 \pm 3) \cdot 10^3$ found experimentally with a recording threshold of 400 is considerably less than the calculated value $N_{DT} = 2 \cdot 10^6$. We note that
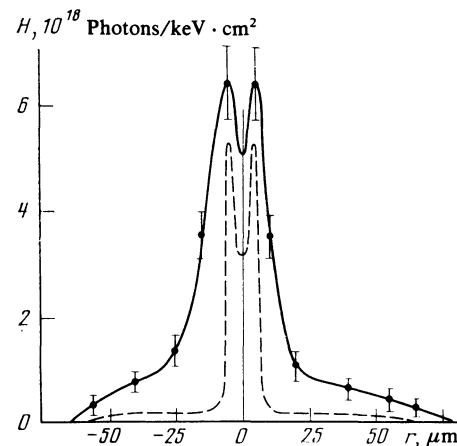

FIG. 2. Analysis of pinhole photographs of the laser plasma recorded using a filter with a central transmission energy $\bar{\varepsilon} = 1.47$ keV (solid trace), $\bar{\varepsilon} = 2.6$ keV (dashed-dotted trace), and $\bar{\varepsilon} = 4.25$ keV (dashed trace).

FIG. 3. Comparison of the experimental (solid) and calculated (dashed) images of the laser plasma for $\bar{\varepsilon} = 2.6$ keV.
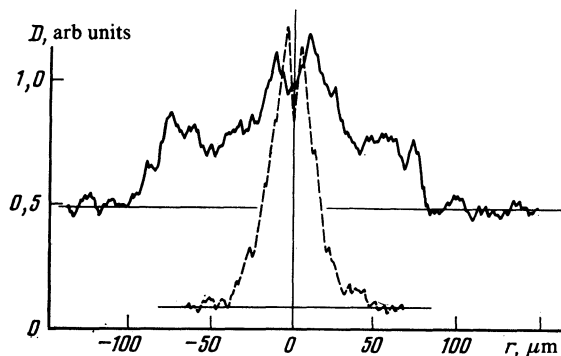
FIG. 4. Comparison of a pinhole laser plasma image recorded for $\bar{\varepsilon} = 1.47$ keV (dashed trace) with a densitogram of the image of the plasma recorded at the wavelength of the w resonance line (solid trace).

the ratio of the experimental and calculated yields was similar in other experiments, in which N_{DT} reached $(0.5-1) \cdot 10^5$. The most likely explanation for the lower experimental yields is that the target compression was not spherically symmetric as was assumed in the calculations.[3]

At the same time, the halfwidth of the central peak in the x-rays images of the laser plasma (Fig. 3) differs considerably—the experimental widths are 2–3 times greater than the calculated values. This broadening may be attributed to the growth of instability as the shell decelerated, particularly in view of the fact that the experimental halfwidth is roughly equal to the radius of the unvaporized portion of the target at the moment the deceleration begins. We also used the sector approximation to estimate the asymmetry of the compression under our experimental conditions and found that the perturbation amplitudes were $\pm(10-15)$ μm for a compressed gas of radius ~ 5 μm.

Figure 7a shows the radial distribution $T_e(r)$ of the electron temperature in the plasma deduced from the ratio of the laser plasma emissivities for continuous x-rays of energy $\varepsilon = 2.6$ and 4.25 keV. The radial distributions of the emissivities were found from the pinhole images by solving an ill-posed inverse problem by the statistical regularization technique[17]; the plasma was assumed to be spherically symmetric and transparent to x-rays at these energies. The experimental time-averaged value $T_e = 0.48 \pm 0.04$ keV at

the center of the plasma[4] was somewhat higher than the calculated value. The time-averaged calculated temperature for the compressed glass was $T_e < 0.36$ keV; moreover, although the DT gas increased T_e to 0.48 keV, it did not contribute appreciably to the x-ray emission from the plasma. The higher experimental value T_e for the compressed glass shell may thus be attributed to mixing of the target material during the deceleration stage.

The above discussion is also supported by Fig. 8, which compares the experimental and calculated time dependences $T_e(t)$ of the electron temperature deduced from the ratio $W(\varepsilon = 0.87$ keV, $t)/W(\varepsilon = 1.25$ keV, $t)$. Indeed, since as noted above T_e is less than 0.3–0.4 keV in the compressed hot glass, the values $T_e(t \approx t_c) \approx 0.6$ keV deduced from the calculated curves $W(\varepsilon, t)$ do not reflect the true temperature of the laser plasma; rather, they indicate that the shell used in the calculation is not optically thin (in the extreme case of an optically dense plasma, the x-rays emission spectrum would be described by a Planck distribution peaking at $\varepsilon = 0.8-1$ keV). However, no increase in T_e for times $\approx t_c$ was noted in the experiment; we conclude that because the compression was not spherically symmetric in the experiment, the plasma remained transparent to photons of energy $\varepsilon = 0.8-1$ keV.

We also used Eq. (1) to calculate the shift of the recombination jump in the continuous spectrum ($\varepsilon_0 = 2.438$ keV) for the plasma temperature and density distributions calculated by the "Zarya" code and obtained a value $\Delta\varepsilon = 110-120$ eV coinciding with the experimental estimate for $\Delta\varepsilon$ (half-maximum). However, the broadening (≈ 10 eV) of the calculated jump is less than the experimental value (Fig. 6). Thus, only the average densities ρ of the compressed glass are similar; the experimental and calculated density profiles are different. The asphericity of the plasma might have contributed to this discrepancy.

3. CALCULATED OPTIMUM VALUES FOR THE "PROGRESS" APPARATUS

The calculated results presented in this paper were found using the "Zarya" code[18] which is based on a one-dimensional two-fluid gasdynamic model, includes terms for various dissipative processes, and treats energy and momentum transfer by nonequilibrium radiation, fast elec-
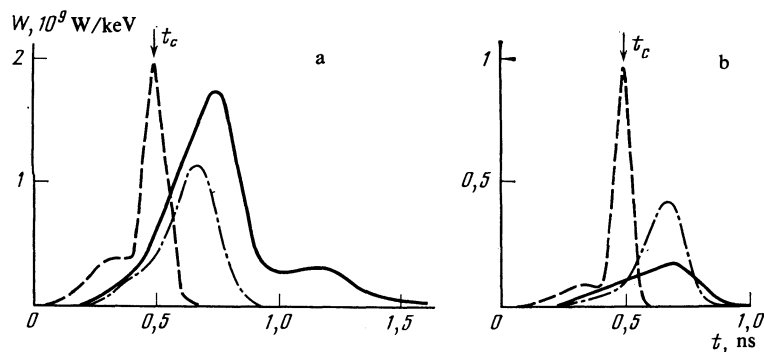

FIG. 5. Time dependence of the x-ray spectral power density $W(\varepsilon, t)$ for $\varepsilon = 0.87$ keV (a) and 1.25 keV (b), recorded experimentally (solid curves) and calculated by the "Zarya" code with (dashed-dotted) and without (dashed) correction for the pulse characteristic of the vacuum x-ray diodes in the recording system.
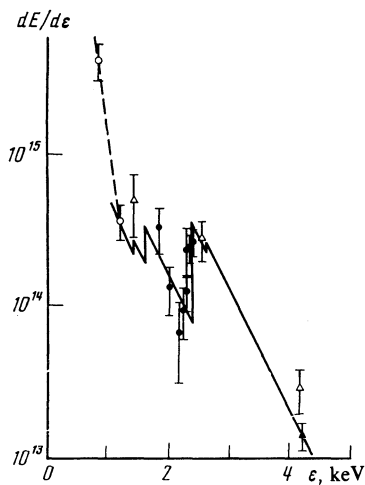
FIG. 6. Measurement results for the continuous x-ray emission spectrum found using vacuum x-rays diodes (O), a crystal spectrometer (△), and semiconductor detector (▲).

trons, and fusion-reaction products. Energy transfer by α-particles and fast electrons can be treated in either the single-group approximation[18] or in the spectral formulation[19] based on the Landau kinetic equation. Nonequilibrium radiative transfer can be treated either in the three-fluid gasdynamic model in Ref. 18 or in the kinetic equation approximation. Both the steady-state and the time-dependent corona[4] models are used to calculate the x-ray absorption and emission coefficients, including the coefficients for the x-ray lines. The x-ray image is calculated with allowance for the resolution of the pinhole cameras.

The "Zarya" code uses a self-consistent model for absorption of the laser radiation which makes it possible to calculate values directly from a knowledge of the laser characteristics, and it includes the principal absorption mechanisms and treats the focusing parameters of the laser light on the target.[20]

The calculations limit electron heat conduction by introducing a maximum flux $q_e^* = f n_e T_e (T_e / m_e)^{1/2}$. We compared the calculated results with data from experiments[4,11,12,13,21] carried out on various equipment for gas-filled glass targets and various laser pulse lengths, energy

flux densities, wavelengths, and focusing conditions. We found that the x-ray spectra, the pinhole images, the fraction of absorbed energy, and the neutron yields calculated by the "Zarya" code agree with the experimental data (the yields agree only for nearly spherical compression). Moreover, the maximum compressions also agree, provided the factor f in the expression for q_e^* obeys the empirical dependence

$$f \approx 0.64 (q \lambda_0^2)^{-0,4}, \tag{2}$$

where q is the energy flux density in 10^{14} W/cm^2 and λ_0 is the laser wavelength in μm.

We used the "Zarya" code to calculate optimum parameter value for maximum neutron yield on the "Progress" device (six beams, lens aperture $F/1.6$, focal spot diameter $d_f = 20$ μm, wavelength $\lambda_0 = 1.06$ μm, peak power $P_L = 0.5$–1 terawatt, Gaussian pulse of duration $\tau_{1/2} = 0.1$–0.2 ns).

In the calculations, P_L and $\tau_{1/2}$ were held fixed and the radius R_0 and wall thickness b of the glass shell were varied. In most of the calculations we took the initial density of the DT gas to be $\rho_0 = 2 \cdot 10^{-3}$ g/cm^3 (the pressure p_{DT} was ≈ 10 atm). The lower bound $0.6 \mu \leqslant b$ was necessary to ensure that the wall of the glass shell was strong enough to withstand pressures $p_{DT} \approx 10$ atm without shattering.

All six beams were assumed to be focused "behind" the target, and the distance a from the center of the target to the focal plane was equal to 3.5 R_0.

The spectral kinetic approximation was used to treat the radiative transfer in the previous calculations discussed in Sec. 2. However, in order to conserve computer time in the optimization calculations, we used the approximation, described in Ref. 18 to handle the radiative transport. This was because test calculations revealed that under our conditions, spectral transfer of radiation has little influence on the neutron yield and gas compression, which are the principal parameters in terms of which the optimization is carried out.

The calculations imply that the minimum admissible shell thickness $b = 0.6 \mu$m is optimal, and the optimum shell radius is given approximately by

$$R_0 = 160 P_L^{0,25} \tau_{1/2}^{0,6} \ [\mu m], \tag{3}$$

$$0.5 \leqslant P_L \leqslant 1 \ \text{TW}, \quad 0.1 \leqslant \tau_{1/2} \leqslant 0.2 \ \text{ns}.$$

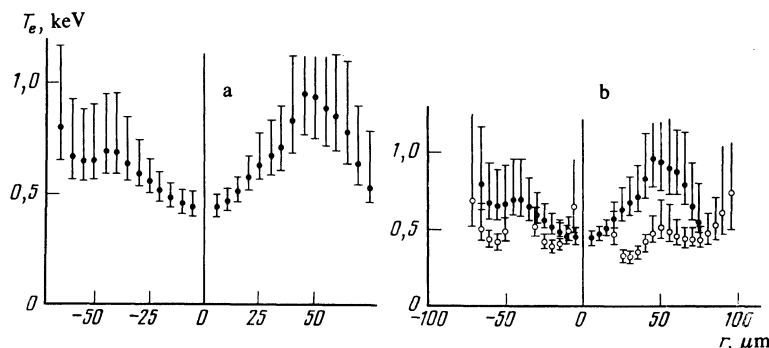The calculated neutron yield for optimum targets was

FIG. 7. Radial electron temperature distributions $T_e(r)$ found by analyzing pinhole images recorded for $\bar{\varepsilon} = 2.6$ and 4.25 keV (●) and images of the plasma at the wavelengths of the Lyman-α line and its dielectronic satellites (O) for experiments No. 78(a) and No. 77 (b).
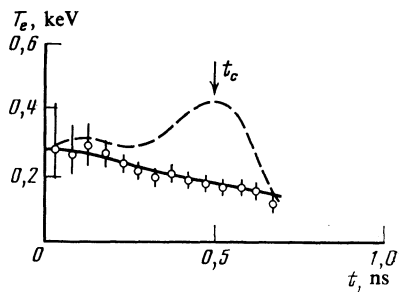
FIG. 8. Time dependence of the electron temperature T_e deduced from the ratio $W(\varepsilon = 0.87$ keV, $t)/W(\varepsilon = 1.25$ keV, $t)$. The solid curve gives experimental values, the dashed curve shows values calculated with allowance for the pulse characteristic of the vacuum x-ray diodes.

$N_{DT} \approx 4 \cdot 10^8 \, P_L^{3.3}$ for compressions $\delta \approx 200 \, P_L^{-1}$, where $0.5 \leqslant P_L < 1$ TW. According to the calculations, δ drops as $\propto \rho_0^{-1}$ when the initial density of the DT gas is increased to $\rho_0 = 4 \cdot 10^{-3}$ g/cm^3 (i.e., the maximum density of the DT gas during the compression is independent of ρ_0), while the neutron yield drops as $N_{DT} \propto \rho_0^{-2/3}$. Under these conditions the optimum target radius is almost independent of ρ_0 for $2 \cdot 10^{-3} \leqslant \rho_0 \leqslant 4 \cdot 10^{-3}$ g/cm^3.

The target must be compressed almost spherically if one is to achieve neutron yields close to the value predicted by the one-dimensional calculations. These are the principal factors responsible for asymmetric compression: variations $\Delta b/b$ in the shell thickness; the fact that the six beams do not reach the target exactly simultaneously; and the nonuniformity $\Delta\Phi/\Phi$ in the illumination of the target surface [$\Delta\Phi/\Phi$ is equal to the intrinsic asymmetry $\Delta\varphi/\varphi$ associated with the irradiation geometry plus $\Delta E/E$, the relative energy spread over the various channels].

According to estimates using the independent sector approximation, the contribution from each of these sources is given by

$$\left(\frac{\Delta r}{r}\right)_{\Delta b} \approx 0.6\frac{\Delta b}{b}\delta^{1/3}, \quad \left(\frac{\Delta r}{r}\right)_{\Delta\Phi} \approx 0.3\frac{\Delta\Phi}{\Phi}\delta^{1/3},$$

$$\left(\frac{\Delta r}{r}\right)_{\Delta t} = \frac{v\Delta t}{2R_0}\delta^{1/3}. \qquad (4)$$

Here the asymmetry $\Delta r/r$ is defined as the deviation of the gas from spherical geometry at the instant of peak target compression. For optimum targets the shell implodes at velocity $v \approx 3 \cdot 10^7$ cm/s, the compression factor is $\delta \approx 200$–300, and the initial target radius is $R_0 \approx 50 \, \mu$m.

We will assume in our estimates that the above asymmetry sources produce a total compression asymmetry given by

$$\frac{\Delta r}{r} = \left[\left(\frac{\Delta r}{r}\right)_{\Delta b}^2 + \left(\frac{\Delta r}{r}\right)_{\Delta\Phi}^2 + \left(\frac{\Delta r}{r}\right)_{\Delta t}^2\right]^{1/2}. \qquad (5)$$

The wall thickness for shells manufactured by current techniques is uniform to within $\Delta b/b \lesssim \pm 2\%$, the energy spread along the channels is $\Delta E/E \lesssim 10\%$, and the beams can be made to strike the target simultaneously to within $\Delta t \lesssim \pm 5$ ps.

Figure 9 shows calculated results for the illumination asymmetry of the target surface for the irradiation configuration in the "Progress" device, assuming all six channels to be identical. More precisely, the nonuniformity $\Delta\varphi/\varphi$ is plotted as a function of the defocusing parameter a/R_0 of the laser radiation. The results found from one-dimensional calculations are also shown for the neutron yield N_{DT}, gas compression δ, laser light absorption factor K, and hot-electron temperature T_h as functions of the focusing conditions for $R_0 = 62.5 \, \mu$m, $b = 0.6 \, \mu$m, $\rho_0 = 2 \cdot 10^{-3}$ g/cm^3, $P_L = 1$ TW, and $\tau_{1/2} = 0.2$ ns. According to Fig. 9, the minimum illumination asymmetry is reached for $a = 4R_0$ and is equal to $\Delta\varphi/\varphi \approx 10\%$. The results in Fig. 9 were calculated for defocusing parameter $a = 3.5R_0$; if a is increased to $(4$–$5)R_0$, N_{DT} drops by a factor of ~ 3 and δ increases by $\sim 20\%$. We note that the illumination asymmetry was calculated by neglecting the refraction of the laser radiation in the "corona" of the target (this refraction should decrease the asymmetry $\Delta\varphi/\varphi$ somewhat). However, one must also bear in mind that the radius of the critical density surface becomes equal to $R_c \approx (1.5$–$2)R_0$ as the laser pulse acts on the target, and this should increase $\Delta\varphi/\varphi$ substantially. However, once R_c appreciably exceeds the initial target radius R_0, the electrons in the corona heat up to ~ 1 keV and the electronic heat conduction should become much more nearly symmetric. According to Ref. 2, the principal contribution to the compression asymmetry comes from the initial
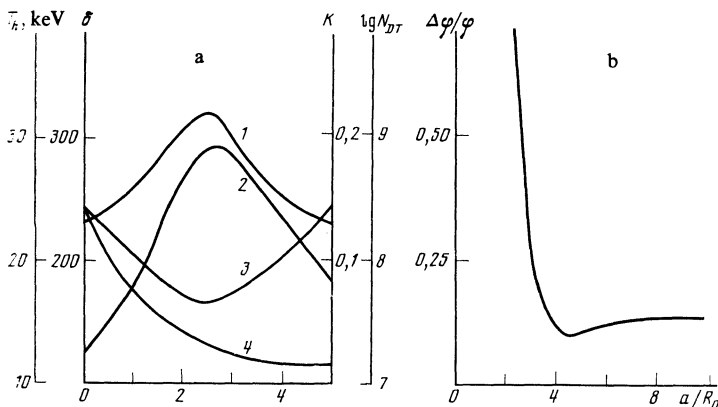

FIG. 9. Calculated parameters as functions of the focusing conditions of the laser radiation on the target: a) absorption coefficient K (curve 1); neutron yield N_{DT} (curve 2); volume compression δ of the DT gas (curve 3); hot-electron temperature T_h (curve 4); b) nonuniformity $\Delta\Phi/\Phi$ of the illumination of a spherical target.

part of the laser pulse; during this stage the corona electrons are still cool, and we can estimate $\Delta\varphi/\varphi$ by using the illumination asymmetry calculated for a target surface of radius equal to the initial value. If we set $\Delta\varphi/\varphi = \pm 15\%$, $\Delta E/E = \pm 10\%$, $\Delta b/b = \pm 1\%$, $\Delta t = \pm 5$ ps, and use (4) and (5), we get the estimate

$$\Delta r/r \approx 0.1\delta^{1/3} \approx 0.6$$

for the asymmetry for $\delta \sim 200$–300. This degree of asymmetry could decrease the neutron yield roughly tenfold.

For optimum targets and $P_L \approx 1$ TW, $\tau_{1/2} = 0.1 - 0.2$ ns we thus anticipate neutron yields N_{DT} of $\approx 10^7$ for compressions $\delta \approx 200$–300 (maximum density $\rho_{\max} \approx 0.5$ g/cm^3) for the "Progress" device with beam focusing behind the target ($a = 4R_0$).

Because laser radiation of short wavelength $\lambda_0 = 0.3 - 0.5$ μm shows the greatest promise for laser fusion,[23] experiments on the "Progress" apparatus using second-harmonic neodymium laser radiation are of considerable interest.

The "Zarya" calculations for $\lambda_0 = 0.53$ μm, $P_L = 0.5$ TW, $\tau_{1/2} = 0.2$ ns, and $a = 3.5R_0$ revealed that the optimum values in this case are $R_0 \approx 75$ μm, $b = 0.6$ μm, and $p_{DT} \approx 10$–20 atm. For these laser and target parameters, the one-dimensional calculation gives $N_{DT} \approx 5 \cdot 10^9$ for compressions $\delta \approx 200$; this yield is two orders of magnitude greater than for $\lambda_0 = 1.06$ μm, $P_L = 0.5$ TW, and $\tau_{1/2} = 0.2$ ns and an order of magnitude greater than for $\lambda_0 = 1.06$ μm, $P_L = 1$ TW, $\tau_{1/2} = 0.2$ ns. Since $\delta \approx 200$ for optimum targets both for $\lambda_0 = 1.06$ μm and for $\lambda_0 = 0.53$ μm, compression asymmetry in these experiments should greatly decrease the neutron yield. Thus, neutron yields of $\approx 10^8$ may be expected for optimum targets in the "Progress" device operating at the Nd second harmonic with an efficiency of $\approx 50\%$.

We note in closing that the neutron yields in our series of experiments agree with the data in Ref. 24, where the laser pulse length was the same as ours, provided we recall that the energy deposition achieved there was ~ 0.2 J/ng. The experimental yield N_{DT} in Ref. 25 was twice as large, but the energy deposition was also greater.

[1] The results of this series of experiments were reported at the Conference on Controlled Fusion and at the Annual Meeting of the Science Council on Plasma Physics held in March 1983 at Zvenigorod.

[2] Provided the implosion of the shell is assumed to be spherically symmetric.

[3] However, the time-integrated pinhole images do not reveal any departure from spherical symmetry.

[4] The electron temperatures at the center of the laser plasma calculated by this method agree with measurements of the radial electron temperature profile found as in Ref. 4 from the ratio of the emissivities for the Ly_α line and its satellites. Figure 7b compares these temperatures for experiment No. 77, for which the conditions were similar to those in experiment No. 78.

[1] A. A. Andreev, A. A. Mak, V. A. Serebryakov et al., Izv. AN SSSR Ser. Fiz. **48**, 2270 (1984).

[2] A. A. Andreev, V. I. Bayanov, V. I. Kryzhanovskiĭ et al., Pis'ma Zh. Tekh. Fiz. **9**, 119 (1983) [Sov. Tech. Phys. Lett. **9**, 53 (1983)].

[3] V. V. Volenko, A. I. Zuev, and A. F. Ivanov, in: Proc. Third All-Union Conference on Laser Optics, Leningrad (1982), p.12.

[4] A. S. Ganeev, A. L. Zapysov, A. I. Zuev et al., Kvantovaya Elektron. (Moscow) **9**, 711 (1982) [Sov. J. Quantum Electron. **12**, 439 (1982)].

[5] A. S. Ganeev, A. L. Zapysov, I. M. Izrailev et al., Prib. Tekh. Eksp., No. 3, 188 (1982).

[6] A. A. Galichiĭ, Yu. A. Mikhaĭlov, G. V. Sklizkov et al., FIAN Preprint No. 120 (1981).

[7] J. S. Pearlman, Rev. Sci. Instrum. **48**, 1064 (1977).

[8] A. L. Zapysov, I. M. Izrailev, V. A. Podgornov et al., Prib. Tekh. Eksp., No. 1, 188 (1982).

[9] A. L. Zapysov, I. M. Izrailev, V. A. Podgornov et al., Prib. Tekh. Eksp. No. 6, 170 (1982).

[10] Yu. A. Kulinich, V. G. Rukavishnikov, Yu. V. Semenov, and M. T. Chineĭkin, Prib. Tekh. Eksp., No. 1, 87 (1973).

[11] Yu. A. Zysin, I. A. Abramov, V. V. Volenko et al., Zh. Eksp. Teor. Fiz. **83**, 1346 (1982) [Sov. Phys. JETP **56**, 773 (1982)].

[12] D. C. Stater, G. E. Busch, G. Charatis et al., Phys. Rev. Lett. **46**, 1199 (1981).

[13] E. Storm, H. G. Ahlstrom, M. J. Boyle et al., Phys. Rev. Lett. **40**, 1570 (1978).

[14] L. P. Presnyakov, Usp. Fiz. Nauk **119**, 49 (1976) [Sov. Phys. Usp. **19**, 387 (1976)].

[15] D. Duston and J. Davis, Phys. Rev. **A21**, 1664 (1980).

[16] C. Lee and A. Hauer, Appl. Phys. Lett. **33**, 692 (1978).

[17] L. S. Turovtseva, IPM Preprint No. OBR-18 (1975).

[18] N. M. Barysheva, A. I. Zuev, N. G. Karlykhanov et al., Zh. Vychisl. Mat. Mat. Fiz. **22**, 401 (1982).

[19] V. A. Lykov and A. A. Chikulaev, IPM Preprint No. 80 (1980).

[20] E. N. Avrorin, A. I. Zuev, N. G. Karlykhanov et al., IPM Preprint No. 77 (1980).

[21] E. Storm, J. E. Swain, H. G. Ahlstrom et al., J. Appl. Phys. **49**, 959 (1978).

[22] N. N. Bokov, A. A. Bunatyan, V. A. Lykov et al., Prikl. Mekh. Tekh. Fiz. **134**, 20 (1982).

[23] E. N. Avrorin, A. I. Zuev, N. G. Karlykhanov et al., Pis'ma Zh. Eksp. Teor. Fiz. **32** 457 (1980) [JETP Lett. **32**, 437 (1980)]; IPM Preprint No. 48 (1980).

[24] E. N. Avrorin, V. A. Eroshenko, S. B. Kormer et al., Zh. Eksp. Teor. Fiz. **87**, 417 (1984) [Sov. Phys. JETP **60**, 239 (1984)].

[25] E. K. Storm, H. G. Ahlstrom, M. J. Boyle et al., Phys. Rev. Lett. **40**, 1570 (1978).

Translated by A. Mason